How Defects Control the Out-of-Equilibrium Dissipative Evolution of a Supramolecular Tubule

How Defects Control the Out-of-Equilibrium Dissipative Evolution of a Supramolecular Tubule

Davide Bochicchio,[a] *Supaporn Kwangmettatam,*[b] *Tibor Kudernac*[b] *and Giovanni M. Pavan*[a,]*

[a] Department of Innovative Technologies, University of Applied Sciences and Arts of Southern Switzerland, Galleria 2, Via Cantonale 2c, CH-6928 Manno, Switzerland

giovanni.pavan@supsi.ch

[b] Molecular Nanofabrication Group, MESA+ Institute for Nanotechnology, University of Twente, PO Box 207, 7500 AE Enschede, The Netherlands

ABSTRACT

Supramolecular architectures that work out-of-equilibrium or that can change in specific ways when absorbing external energy are ubiquitous in nature. Gaining the ability to create *via* self-assembly artificial materials possessing such fascinating behaviors would have a major impact in many fields. However, the rational design of similar dynamic structures requires to understand and, even more challenging, to learn how to master the molecular mechanisms governing how the assembled systems evolve far from the equilibrium. Typically, this represents a daunting challenge due to the limited molecular insight that can be obtained by the experiments or by classical modeling approaches. Here we combine coarse-grained molecular models and advanced simulation approaches to study at submolecular (<5 Å) resolution a supramolecular tubule that breaks and disassembles upon absorption of light energy triggering isomerization of its azobenzene-containing monomers. Our approach allows us to investigate the molecular mechanism of monomer transition in the assembly and to elucidate the kinetic process for the accumulation of the transitions in the system. Despite the stochastic nature of the excitation process, we demonstrate how these tubules preferentially dissipate the absorbed energy locally, *via* the amplification of defects in their supramolecular structure. We find that this constitutes the best kinetic pathway for accumulating monomer transitions in the system, which determines the dynamic evolution out-of-equilibrium and the brittle behavior of the assembly under perturbed conditions. Thanks to the flexibility of our models, we finally come out with a general principle, where defects explain and control the brittle/soft behavior of such light-responsive assemblies.

KEYWORDS: supramolecular polymers, self-assembly, out-of-equilibrium, stimuli responsive, defects, coarse-grained martini force-field, azobenzene

Nature uses self-assembly to create supramolecular materials that absorb external energy and transduce it into dynamic functions with great fidelity.[1,2] Such fascinating behavior is deeply encoded at the molecular level, typically into building blocks (or monomers) that undergo structural transformations in response to specific stimuli. The molecular transformations are subsequently transmitted and amplified at the supramolecular level inducing a dynamic response of the assembly. Prototypical examples are cellular microtubules, which can convert chemical energy into mechanical forces that are key for the motion or shape-shifting of cells.[3,4] GTP binding and subsequent hydrolysis induces a series of conformational changes in the tubulin building blocks of these tubular assemblies controlling their dynamic polymerization and depolymerization.[5,6] But the examples of supramolecular systems that can convert external energy into a dynamic adaptation (or response) are ubiquitous.[1,7–9]

In the recent years synthetic chemists put a considerable effort into designing artificial systems that work in similar way.[1,10–17] One way is to use chemical energy (*e.g.*, intermolecular interactions, molecular fuels, *etc*.) to drive the system out of equilibrium.[18] Another typical strategy is to introduce light-responsive molecular actuators in the self-assembling monomers that undergo transitions when stimulated. In this family, a well-studied example is azobenzene, a photo-responsive molecule switching between *trans* and *cis* isomers when irradiated with light.[19] Such molecular switches have been incorporated into self-assembling monomers to obtain various types of stimuli-responsive supramolecular structures.[16,20–24]

While chemically- and light-stimulated supramolecular systems present some differences (*e.g.*, microscopically reversible *vs.* light-activated excited states),[25–27] in general in these systems the assembly is driven away from the equilibrium by the absorption of external energy and this

dynamically reacts, or adapts, evolving toward a new equilibrium state. In all cases, how exactly these perturbed systems evolve in time under such non-equilibrium conditions is difficult to predict and control. A major limitation is that the design of such stimuli-responsive systems typically proceeds *via* trial-and-error approaches. Furthermore, while in artificial settings the supramolecular systems are typically studied at the level of statistical ensembles or, in the best case, of individual self-assembled objects, this does not suffice for a molecular understanding of the mechanisms determining their behavior. To mimic the great fidelity of natural materials in achieving dynamic functions it is necessary to understand the molecular factors and mechanisms that control how the monomer transitions are transduced into a specific dynamic evolution of the self-assembled system. This requires exploring the evolution of the assembly while this is out-of-equilibrium at a submolecular resolution. While this is experimentally daunting, molecular simulations provide useful molecular insight into such supramolecular materials[28–35] and their stimuli-responsive behavior.[36–39] For example, azobenzene-containing supramolecular structures – *e.g.*, monolayers,[40] nanoparticles,[22,41,42] vesicles,[24] tubules,[23] liquid crystals,[43,44] *etc.* – have been studied by means of quantum mechanics/molecular mechanics (QM/MM),[40] all-atom (AA)[22,23] and coarse-grained (CG)[41,45] simulation approaches. Such efforts provided molecular-level insight into the structure of assemblies. However, exploring the molecular processes underpinning the dynamic evolution of a perturbed assembly under the influence of the stimulus remains a challenge.

As a representative case, here we focus on supramolecular tubules containing azobenzene units in the hydrophobic V-shaped tails of their self-assembling monomers. Previous experimental work has shown that these tubules first break into shorter segments and then disassemble upon UV-light exposure in the timescale of minutes/hours (**Figure 1**).[23] Considering the stochastic nature of the

UV-light excitation of the azobenzene units in the system, the non-equilibrium dynamic behavior of these tubules – breaking into segments instead of uniformly melting/disassembling in time – is interesting. This suggests an intrinsic preferential way for these self-assembled tubules to evolve dynamically while they absorb energy from light.

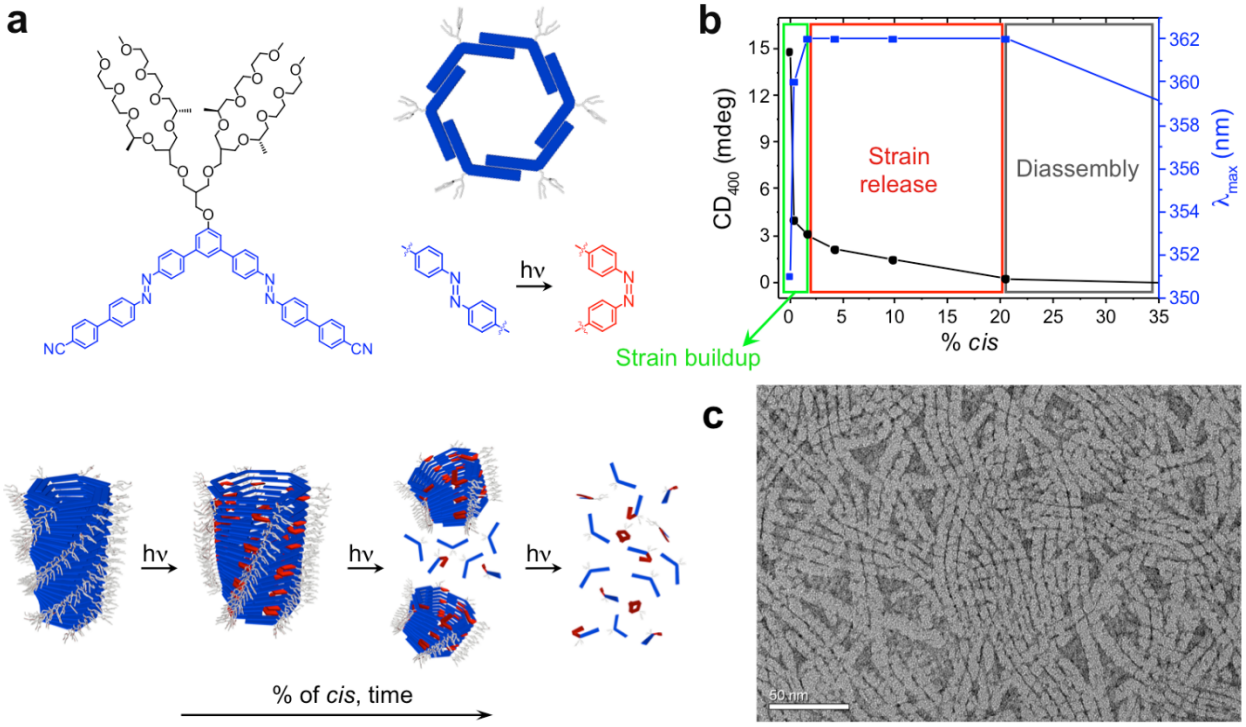

Figure 1 Photo-responsive breakage and disassembly of supramolecular tubules.[23] **a** Structure of the monomers: these hierarchically self-assemble in water into rings and tubules due to hydrophobic interactions, π-π stacking and shape recognition. Bottom scheme: UV light-triggered isomerization of the azobenzene units in the hydrophobic monomer tails triggers strain accumulation, breakage and disassembly of the tubules.[23] **b** Previous experiments: CD intensity at $\lambda = 400$ nm (black) and position of λ_{max} (blue) during the light exposure (monomer concentration 2.5 μM), expressed as a function of the percentage of *cis* in the system. Three phases of strain buildup/conformational change (green), strain release/tubule breakage (red) and disassembly (grey) are identified.[23] **c** Stained TEM image of the tubules (see also **Supporting Figure S1**).

Here we combine fine coarse-grained models with advanced simulation approaches to investigate the molecular factors controlling the pathway undertaken by the perturbed tubules during their dynamic evolution toward disassembly. The submolecular (<5 Å) resolution of our

models allows us to link the mechanism and kinetics of the molecular transitions with the defects generated in the supramolecular structure and the dynamic evolution of the perturbed assembly. We demonstrate how defects accumulate on the tubules and dissipate the absorbed energy according to a precise kinetic mechanism, which origin is deeply encoded at a molecular level. These results provide us a deep comprehension of the key factors controlling how such assemblies evolve when they are perturbed by light.

Results and discussion

Monomer isomerization in the supramolecular tubule. Investigating the UV-light activated *trans*-to-*cis* transition of the azobenzene groups of the monomers inside the self-assembled structure is a first key step to understanding how the transitions affect the assembly and produce a dynamic response in these tubules. The great complexity of this supramolecular system exceeds the possibilities of fully atomistic (AA) models (see Methods for details). At the same time, this required the development of a coarse-grained (CG) model for the monomers of **Figure 1** fine enough to reproduce the trans-to-*cis* azobenzene isomerization in accurate way (mechanism and pathway).

The trans-to-*cis* azobenzene isomerization occurs out-of-plane, mainly *via* a rotational mechanism involving the first excited state of *trans* azobenzene (*S**) and the torsion of the central N–N bond.[46–48] First, we developed an AA model for the monomers reproducing the azobenzene *trans*-to-*cis* transition accurately (**Figure 2: AA$_{S^*}$**). In model **AA$_{S^*}$**, the central CNNC dihedral potential term of the azobenzene tails was changed from the native black curve (unperturbed *trans* azobenzene) into the blue one of **Figure 2a** (*S**: excited *trans* azobenzene). In this way, the excited

tails undergo spontaneous *trans*-to-*cis* isomerization following the correct pathway[46,47] (**Figure 2a-d**) during an **AA*S**-MD simulation (see Methods).

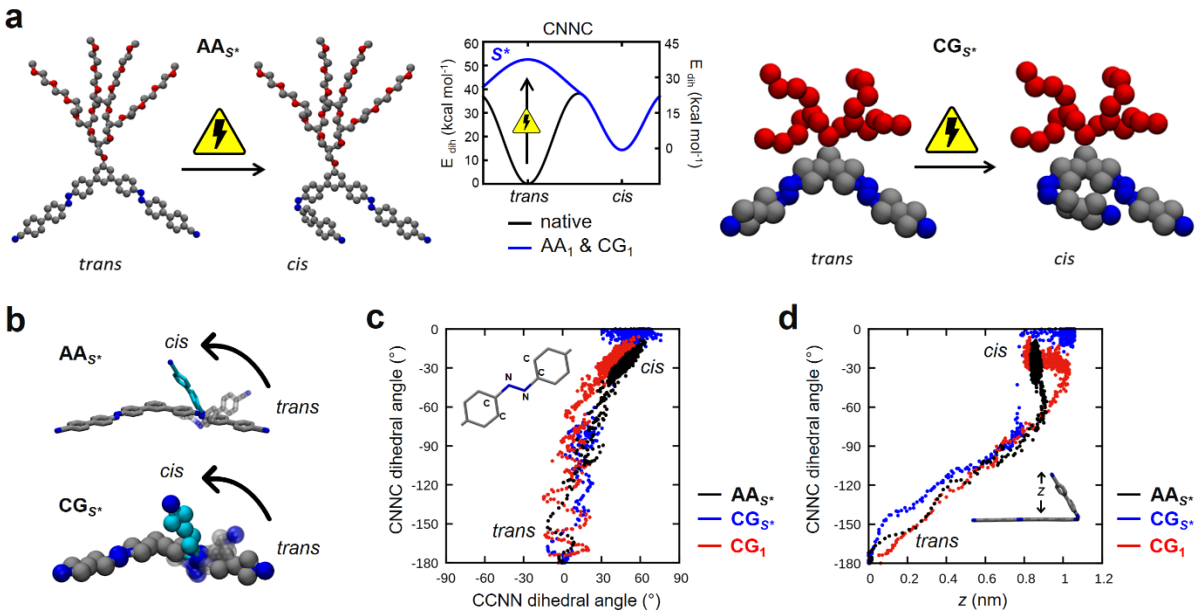

Figure 2 CG models for the *trans*-to-*cis* isomerizing monomers. **a** AA and CG models for the photo-responsive monomers. The switching of tails is obtained by replacing the native CNNC dihedral potential (black curve) with a potential (blue) in which the *trans* conformer becomes the new maximum (consistent with the first excited state of azobenzene, *S**) and the *cis* conformer the new minimum. **b** The CG models used in this work are optimized to reproduce the *trans*-to-*cis* isomerization pathway of **AA*S***. **c,d** *Trans*-to-*cis* isomerization MD trajectories as a function of the CNNC dihedral angle and of (**c**) the CCNN one or of (**d**) the out-of-plane *z*-height. All trajectories follow the correct rotational *trans*-to-*cis* transition pathway.[46,47]

Model **AA*S*** was used as a reference to develop a consistently accurate CG model (**Figure 2: CG*S***) allowing us to study the system on a larger-scale (structure and dynamics). Model **CG*S*** was optimized to reproduce the strength of the monomer-monomer interaction/stacking (**Supporting Figure 2**) and the *trans*-to-*cis* isomerization pathway of model **AA*S*** (see Methods). The *trans*-to-*cis* isomerization trajectory obtained from the MD simulations (rotational pathway) is the same in models **AA*S*** and **CG*S*** (**Figure 2c**: black *vs.* blue). The monomer tails also complete their transition at the same out-of-plane height in all models (**Figure 2d**). This is crucial

in our case, as the out-of-plane character of the monomer transitions is key for the impairment generated in the stacked structure of these supramolecular tubules.

We built a CG model for the self-assembled tubule (**Methods**). This models a section ~80 nm long of the bulk of an infinite tubule solvated in water (**Figure 3a**). This is already in the range of what is observable by cryo-TEM (see **Figure 1c**), while the resolution of our CG model is <5 Å. This model was preliminarily equilibrated *via* CG-MD, showing the great stability and highly ordered tubular structure under unperturbed (before irradiation) conditions (Methods and **Supporting Figure 3**).

Isomerization of the monomer tails inside the tubule occurs in a highly crowded environment. We used well-tempered metadynamics (WT-MetaD)[49] simulations biasing the *trans*-to-*cis* transition of one tail in a monomer to obtain information on the free-energy barrier for this isomerization process in assembled vs. disassembled state (Methods). For a disassembled unperturbed monomer, the tail transition from *trans* to *cis* configuration requires to overcome a free energy barrier of ~35-40 kcal mol^{-1} (**Figure 3b**, dotted black) – that corresponds, essentially, to the native barrier in the CNNC dihedral potential of **Figure 2a** (black curve). However, for a monomer incorporated in the perfect all-*trans* tubule the transition barrier is much higher (**Figure 3b**, red: ΔG ~70 kcal mol^{-1}). This is the effect of crowding in the assembled structure, which stabilizes the *trans* (planar) conformation of the monomer by an additional ~25-30 kcal mol^{-1}.

This has strong consequences. For example, in a disassembled monomer where one azobenzene tail is described by model **CG$_{S^*}$** (**Figure 2a**, blue), the excited tail undergoes fast spontaneous *trans*-to-*cis* isomerization in the timescale of picoseconds (~10^{-12}–10^{-11} s on average), consistent with the kinetics expected for the process.[40] However, in the case of excitation of one single monomer tail (**CG$_{S^*}$**) inside the tubule while the other ones are unperturbed, we could not observe

the transition of the excited tail within microseconds of **CG*S**-MD simulation. This is consistent with recent studies showing that azobenzene isomerization may be even impeded in crowded environments such as, for example, in dense nano-grafted azobiphenyl monolayers[40,50–53] or in confined cages.[54] Under such conditions, the considerable constrain introduced by monomer packing in these tubules makes the isomerization of an excited *S** *trans* tail a rare event within the timescale accessible by our **CG*S**-MD simulations.

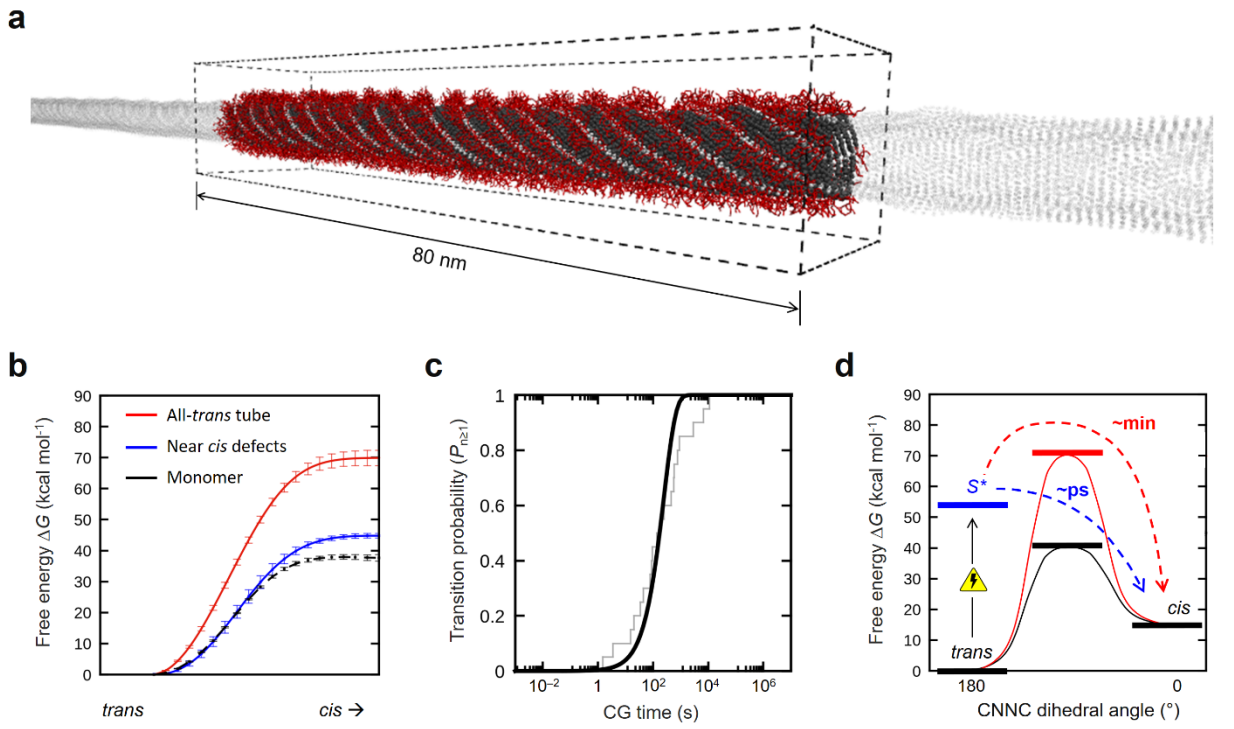

Figure 3 *Trans*-to-*cis* azobenzene isomerization in the self-assembled tubule. **a** Equilibrated CG model for an infinite supramolecular tubule. The V-shaped tails (initially, all-*trans*) are colored in grey, hydrophilic PEG chains are colored in red, the simulation box is shown as dotted lines, water is not shown for clarity. In the periodic images of the tubule, only the V-shaped tails are shown as light-grey shadows. **b** Free energy barriers obtained from WT-MetaD simulations for the transition of one *trans* tail to *cis* in a perfect all-*trans* tubule (red), close to already transited *cis* tails (defects) in the tubule (blue) and in an isolated/disassembled monomer in water (dashed black). Error bars in the plots represent s.e.m. **c** Transition time distribution for the isomerization of an excited *trans* tail (**CG*S***) in a perfect tubule obtained *via* multiple infrequent WT-MetaD simulations (each grey segment in the distribution is one WT-MetaD run). The Poisson distribution fitting curve providing the characteristic timescale for the event (τ) (see **Methods**) is shown in black. **d** Scheme: thermodynamics and kinetics of the *trans*-to-*cis* tail transition in a perfect tubule (red) *vs.* in a disassembled/free monomer (blue).

As recently used for studying rare monomer exchange transitions in supramolecular polymers,[32] we ran multiple infrequent WT-MetaD[55] simulations activating the transition to *cis* of one excited *S* trans* tail (**CG*S**) in a tubule where all other tails are unperturbed. The transition times collected from these biased simulations were used to reconstruct the Poisson transition probability distribution (**Figure 3c**: Pn≥1) and the characteristic timescale (τ) for the real (unbiased) transition event (see Methods for details).[32,56] While it is clear that the transition of a *S* trans* tail to *cis* in our model of a perfect tubule does introduce a defect in the assembly, the τ obtained for such event is found in the order of minutes (~10^1–10^2 s).

We used the same WT-MetaD approach to investigate the characteristic timescale for the transition to cis of excited *S* trans* tails that are in the immediate neighborhood of already present cis defects (see Methods). We could observe that in such a case, where the transition pathway is almost free from steric hindrance, the free-energy barrier for the transition becomes similar to that of a disassembled monomer (**Figure 3b**, blue curve, ~45 kcal mol^{-1}). Consistently, the tail transition to *cis* also occurs in the timescale of tens/hundreds of picoseconds (~10^{-11}–10^{-10} s). As summarized in the scheme of **Figure 3d**, this is due to the fact that in the presence of a defect the native barrier to the transition generated by the crowding (order) in the assembly is strongly reduced. This makes the transition of excited *trans* tails (*S**) ~10^{-12} times statistically more probable/frequent close to already transited *cis* tails (defects) rather than in other regions of these tubule where the tails are all trans.

While these reconstructed kinetics are obtained from a simplified CG model and has qualitative/comparative meaning, the difference between the two cases is prominent. In fact, even considering the stochastic character of the excitation process in the real system, the probability of exciting one tail that is exactly closest neighbor to a hypothetic first *cis* one is just below ~1/2000

in our tubule model (containing 1080 monomers and 2160 azobenzene tails) and ~1/20000 in a real tubule (maximum size ~1 μm, ~10000 monomers). Despite this statistical penalty (~10^{-4}–10^{-3}), the effect of crowding is still orders of magnitude stronger. Based on this approximated calculation, the relative probability of having a transition close to a defect rather than in ordered domains of the tubule is very large (~10^{8}–10^{9} more likely/frequent). Moreover, it is worth noting that such a strong kinetic asymmetry in favor of accumulating *cis* tails in spatially correlated instead of random way is obtained from simulations where the excited *trans* tail cannot de-excite back in the models. However, the lifetime of the excited state S* of *trans* azobenzene is in the order of picoseconds,[40,57] and in the real system the de-excitation to the ground state of tails excited in perfect regions of the tubule is a likely event. Thus, the strong kinetic tendency to accumulate *cis* tails in a spatially correlated way leading to defects amplification could be at worst underestimated by our model. Nonetheless, the analysis of our infrequent WT-MetaD simulations demonstrates that, in general, in this system the transitions most likely occur in correspondence of the defects that are created or that may be intrinsically pre-existing along these tubules. This is coherent with a mechanism of accumulation of the transitions in the system leading to the amplification of local defects, which tend to grow in size rather than in number on the structure of the tubule. This is consistent with the experimental evidence that these tubules do not melt or uniformly disassemble upon UV-light irradiation, but they break locally into long-lived segments which then disassemble on a longer timescale.[15]

Effect of monomer transitions on the supramolecular structure. Modeling the stochastic nature of photo-activated monomer transitions that accumulate on the experimental timescale of minutes exceeds the possibility of MD simulation. In such a slow process, the assembly has

sufficient time to relax and equilibrate while the percentage of *cis* tails increases in the system. Thus, to obtain a reliable picture of the effect of the *trans*-to-*cis* transitions on the supramolecular structure, we opted for equilibrating the tubule at various percentages of *cis*. From a first **CG$_{S^*}$**-MD simulation where all tails in the system were excited to undergo transition, we extracted configurations for the tubule at 2.5%, 5%, 10%, 15%, 20% and 30% of cis. Interestingly, also in this case we could observe that the *cis* transitions do not appear randomly but as spatially correlated in the tubule, consistent with the kinetic data discussed above (Methods). Equilibrating the tubule at these fixed *cis* percentages allowed us to study how this relaxes under a condition where the *trans*-to-*cis* transitions accumulate on a longer timescale (as in the experiments).

Below 5% of cis, we could observe local deformations of the tubule structure (**Supporting Figure 4**). Between 10% and 15% of *cis* the supramolecular structure was seen to become unstable. At 15% of *cis* the tubule started breaking in correspondence of cis-rich domains (defects) after a few microseconds of CG-MD (**Figure 4a**). At 30% of cis, while the tubule broke into shorter segments, we could clearly observe the spontaneous disassembly of monomers leaving the tubule during the equilibration CG-MD (**Supporting Figure 4**). These results are consistent with the experimental evidence, indicating structural destabilization of the real tubules starting from below ~10% of *cis* and disassembly from ~20% of *cis* in the system. This proves the reliability of our models. In fact, it is worth noting that in these simulations we are not biasing the exchange of monomers out from the tubule, while the disassembly of *cis* monomers (a non-assembling species) is a spontaneous event occurring on longer timescales than the monomer transitions.

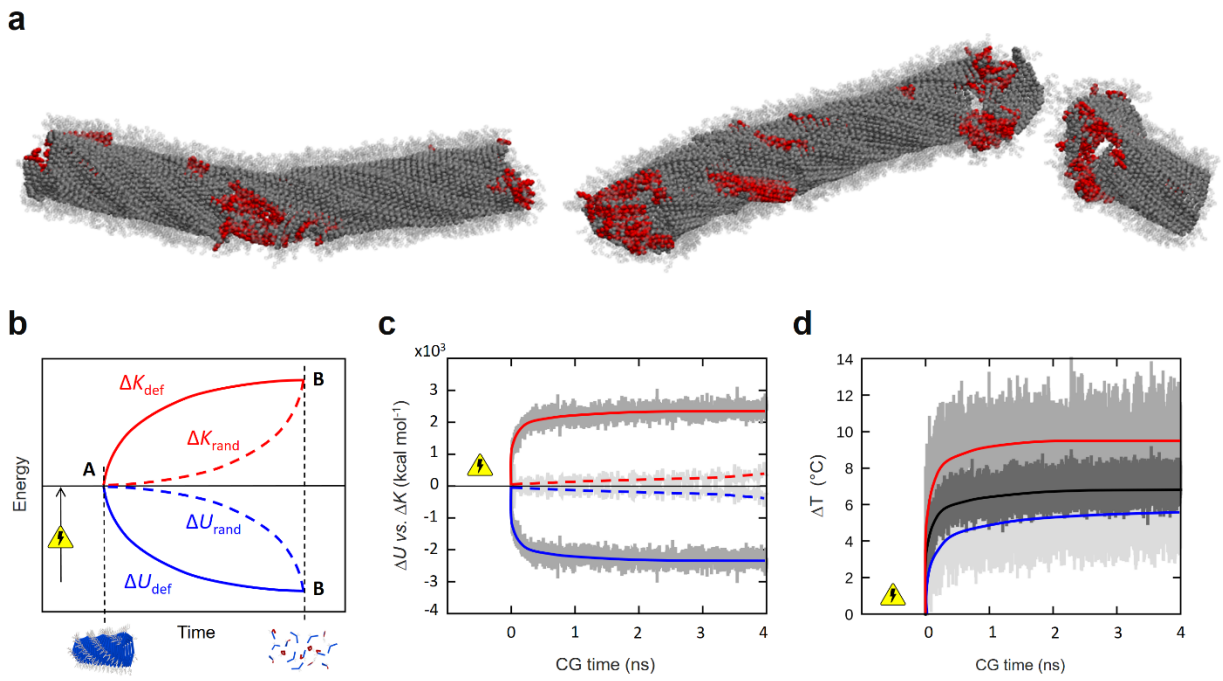

Figure 4 Effect of the monomer transitions on the tubule. **A** Tubule at 15% of *cis* after 10 μs of equilibration CG-MD: *trans* tails are colored in grey, *cis* tails (defects) in red, hydrophilic PEG chains are represented as light grey shadows (water not shown for clarity). **B** Scheme for energy conversion in a simplified perturbed system: the irradiated tubule, brought far from equilibrium by UV-light (state A), evolves in time toward a new equilibrium state where the monomers are disassembled (state B). Among the pathways that the system can take to evolve from A to B, the conversion of the absorbed energy into kinetic energy proceeds faster at each time step when the *cis* transitions appear as spatially correlated (amplification of local defects, solid lines) rather than when these accumulate randomly on the tubule structure (dotted lines). **C** Conversion of potential energy (ΔU) into kinetic energy (ΔK) in the system as a function of the simulation time after the transition of a first *cis* tail in the tubule (all energy variations are calculated respect to this reference point, set to 0). **D** Energy dissipation: increase of temperature (ΔT, red) and decrease of inter-monomer interaction energy in the system (ΔE, blue). Grey shadows are the native data obtained from the NVE CG-MD simulations of a tubule at 5% of *cis* (see **Methods**).

Dissipative dynamic behavior of the perturbed tubules. We investigated further the deep origin for the out-of-equilibrium behavior of these tubules. When the equilibrated tubules absorb energy from UV-light, these are brought far from equilibrium (in a new thermodynamic state A: excitation), producing the evolution of the system toward a new equilibrium state (state B: disassembly). In our **CG*S**** models, the absorbed energy appears as a penalty (bias) on the CNNC

dihedral term of the potential energy of the tubule – an energetic burden that is released when the excited tails isomerize into *cis* conformation). We started from the hypothesis that among the (infinite) possible pathways to move from A to B, the tubule will take that allowing for the fastest (maximal) dissipation of the absorbed energy in time, while in the system considered as a whole the energy dissipated by the assembly is dynamically converted into something else.

In the real system the energy absorbed by the tubule depends on the number of tails that are effectively excited by UV-light (which may vary with time). However, let us consider a simplified scenario, where a fixed amount of energy is absorbed bringing the system far-from-equilibrium (state A). Based on our kinetic analysis (WT-MetaD), it is interesting to compare two hypothetical extreme pathways, among all possible ones, that the tubule can take to evolve from state A (excited tubule) to state B (disassembly). These are illustrated in the conceptual scheme of **Figure 4b**. In one case the *cis* tails accumulate in a spatially correlated way, leading to the amplification of local defects on the assembly (solid curves). In the second case the transitions appear randomly on the tubule structure (dotted curves). Overall, the absorbed energy is the same in all cases and at regime (on an infinitely long timescale) all pathways would converge to the same state (B). However, our WT-MetaD results indicate that the first case would allow the tubule to get rid of the energetic penalty provided by UV-light excitation (ΔU_{def}, solid blue) faster compared to the second case (ΔU_{rand}, dotted blue). While the absorbed energy leaves the tubule in time, in the system considered as a whole this does not leave but is transformed ($E = U + K$ = cost.), inducing the dynamic evolution of the system. In particular, to a change in the global potential energy (ΔU: release of absorbed energy) of the system corresponds a change in kinetic energy (ΔK: system evolution) over time. The variation in kinetic energy in the system would be thus consistently faster in the case of spatially correlated vs. random defects (red ΔK_{def} vs. ΔK_{rand} curves).

We designed in silico experiments to challenge this concept. We compared two tubule models where 5% of tails are excited and can undergo transition to *cis* as randomly distributed on the structure *vs.* spatially correlated into local defects. The energy (bias) globally provided for the transitions and the total energy (E) is the same in both systems, while the unique difference is the distribution of the excited tails on the tubule (Methods). We ran CG-MD simulations for these systems in NVE conditions, where the total energy of the systems is constant during the runs. **Figure 4c** shows the conversion of ΔU into ΔK in the two systems. The results clearly demonstrate that, starting from state A, the conversion of ΔU_{def} into ΔK_{def} is faster than that of ΔU_{rand} into ΔK_{rand}. In the former case the excited *S* trans* tails undergo transition quickly in the system (consistent with what is seen in our WT-MetaD simulations). Conversely, the transitions take longer time to accumulate when these occur randomly – in the same timescale ΔU_{rand} and ΔK_{rand} barely deviate from 0 (**Figure 4c**: dotted red and blue lines). Consistent results have been obtained also for 10% or 15% of spatially correlated vs. random excited tails in the tubules.

Noteworthy, the ΔU and ΔK (**Figure 4**) are those of the whole system (solute plus solvent). However, the ΔU change is related to the tubule only – *i.e.*, to the release of the energetic dihedral bias by the transiting tails. On the other hand, the measured ΔK accounts for the change in kinetic energy of the tubule (dynamic breakage/evolution) plus that of the solvent (energy dispersion). In these NVE simulations the systems are not thermalized, which allowed us to measure the variation of temperature of the systems during the runs (ΔT). The ΔT increases in time faster in the case of localized than in random defects (**Figure 4d**, black), consistent with the ΔK data. The global ΔT of the systems is initially due to an increase of temperature of the tubule (**Figure 4d**, red: ΔT_{tube}, associated to the increase ΔK of the transiting tails). However, it worth noting that with a small delay the temperature of the solvent also increases (**Figure 4d**, blue: ΔT_{water}). This demonstrates

that part of the energy initially absorbed by the tubule is transferred to the surrounding and dissipated as heat. Such a preferential way for this assembly to evolve out-of-equilibrium along the dynamic pathway allowing for the fastest dissipation of absorbed energy (local defects amplification) explains why these tubules break rather than uniformly dissolving in time upon UV-light irradiation.[23] In a broader sense, such innate behavior reminds the dissipative adaptation seen in other supramolecular structures generated *via* chemically-driven self-assembly.[58–61] While these systems are different from the light-activated tubules studied herein,[25–27] they have some points in common, although the theoretical interpretation of their out-of-equilibrium behavior is still at the center of intense scientific discussions.[58,62] Typically, in such systems the assembly of monomers is not spontaneous, but it is driven by the consumption of external energy or of a molecular fuel (consumed energy: $E \neq 0$). When the energy influx (*i.e.*, the trigger to self-assembly) changes ($\Delta E \neq 0$), such systems adapt dynamically evolve following to the dynamic pathway that guarantees the fastest dissipation (or conversion) of energy in time. While in our case the monomers self-assemble spontaneously into tubules and do not require energy for this process ($E = 0$), the energy provided by the excitation of the tails ($\Delta E \neq 0$) triggers a similar dynamic response/evolution of the assembly.

Energy dissipation through defects and dynamic evolution of the tubule. To generalize and further demonstrate this concept, we developed a simplified dynamic "toy model" for the system (**CG$_1$**). Model **CG$_1$** reproduces the correct out-of-plane isomerization pathway of the excited monomer tails of **AA$_{S^*}$** and **CG$_{S^*}$** (**Figure 2c,d**,red). However, in this case a reduced bias is provided to all *trans* tails in the tubule to undergo transition during a **CG$_1$**-MD simulation. The bias was optimized to reproduce the same average structural and energetic impairment in the tubule

obtained by equilibrating it at various *cis* percentages (see Methods). In this sense, model **CG$_1$** does not aim anymore at reproducing the precise physics of the monomer transitions in the assembly, but it is rather a phenomenological model in that it reproduces the average effect on the tubule of monomer transitions accumulating on a slow timescale. Model **CG$_1$** allows observing the dynamic evolution of such a simplified version of the system at a resolution <5 Å (**Supporting Movie 1**). The behavior of the perturbed tubule observed during the **CG$_1$**-MD run (**Figure 5a**) is globally consistent with the static pictures obtained by equilibrating the tubule at the different percentages of *cis* as described above (**Supporting Figure 4**).

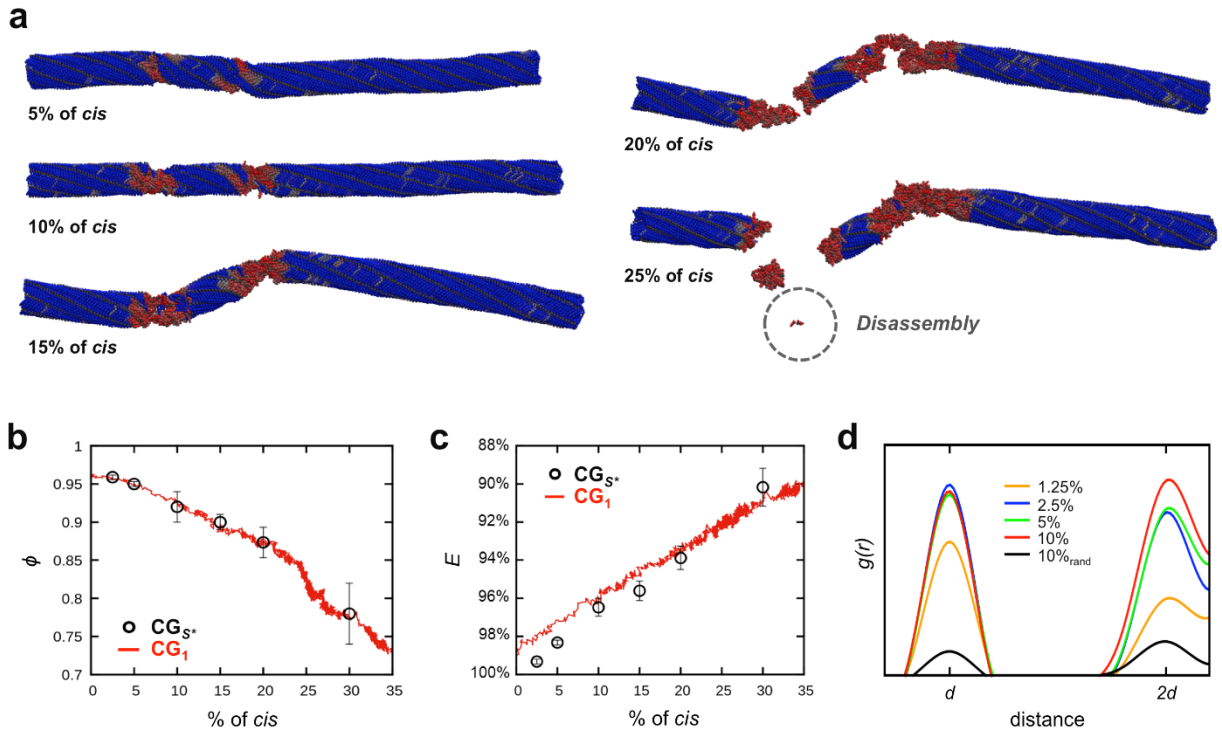

Figure 5 Evolution of the tubule during the *trans*-to-*cis* monomer transitions. **a** Snapshots of the tubule at various percentages of *cis* taken from the **CG$_1$**-MD simulation (*trans* and *cis* tails are colored in blue and red, oligoether chains and water not shown for clarity). **b** Decrease of order (ϕ) in the assembly as a function of the *cis* percentage (ϕ=0.96 in the native equilibrated tubule) during the **CG$_1$**-MD run (red line) or equilibrating the tubule at various *cis* percentages (black points). **c** Loss of monomer-monomer interaction energy *E* (in percentage, respect to the unperturbed tubule) as a function of the *cis* percentage (dynamic **CG$_1$**-MD run in red; tubule equilibrated at various *cis* percentages, black points). Error bars in the black data represent s.e.m. **d** Defects correlation and amplification: radial distribution functions (*g(r)*) of *cis* tails at different *cis* percentages obtained from the **CG$_1$**-MD run. The *g(d)* and *g(2d)* peaks (d: distance between

closest neighbor tails in the stack) indicate a high probability of transitions occurring close to other *cis* tails: defects correlation and amplification. Black *g(r)* curve: 10% of randomly displaced *cis* reported for reference.

The red curves of **Figure 5b,c** show the evolution of the ϕ and E parameters as the *cis* percentage increases in the tubule during the **CG$_1$**-MD run, which intercept the black points obtained from the CG-MD equilibration runs at the different percentages (see Methods).

It is worth noting that this case we are providing the same bias to all tails in the system for the transitions. This is like giving an energy bath to the whole assembly. While in such a case the excitation of the monomers is homogeneous, still the *cis* tails do not appear randomly on the tubule but rather as localized into defects during the **CG$_1$**-MD run (**Figure 5a**, in red). The radial distribution functions (*g(r)*) of the *cis* tails in the tubule demonstrate strong spatial correlation between the generated defects emerging early during the **CG$_1$**-MD run, when the *cis* percentage is still very low in the system. Shown in **Figure 5d**, the first *g(d)* peak (d: stacking distance between neighbor tails in the native tubule) indicates a very high probability to have *cis* transitions occurring close to other *cis* tails (defects correlation) already when the number of transitions is very low (the *g(r)* for a random distribution of 10% of *cis* is reported in **Figure 5d** in black for reference). The second peak (*g(2d)*) demonstrates the strong tendency in the system to enlarge existing defects (defects amplification) rather than creating new ones on the tubule structure.

From the **CG$_1$**-MD simulation we calculated the interaction energy of each tail with the other ones in the assembly. The plot of **Figure 6a** shows that at 2.5% of cis, two *cis* domains are visible in the tubule (red dots), while the average interaction energy of the *cis* monomers is decreased respect to the *trans* ones. The same analysis conducted on the tubule at 5% and 25% of *cis* shows the amplification of the two *cis* domains (**Figure 6b-c**). Interestingly, while in these cases the *trans* monomers tend to preserve their interactions, the energy of the *cis* tails is found less and less

favorable as their percentage increases in the system (insets). This fits well with the non-assembling nature of the *cis* monomers – at 25% of *cis* there are *cis* monomers spontaneously leaving the assembly (**Figure 5a**: black circle; **Figure 6c**: red point with interaction energy zero).

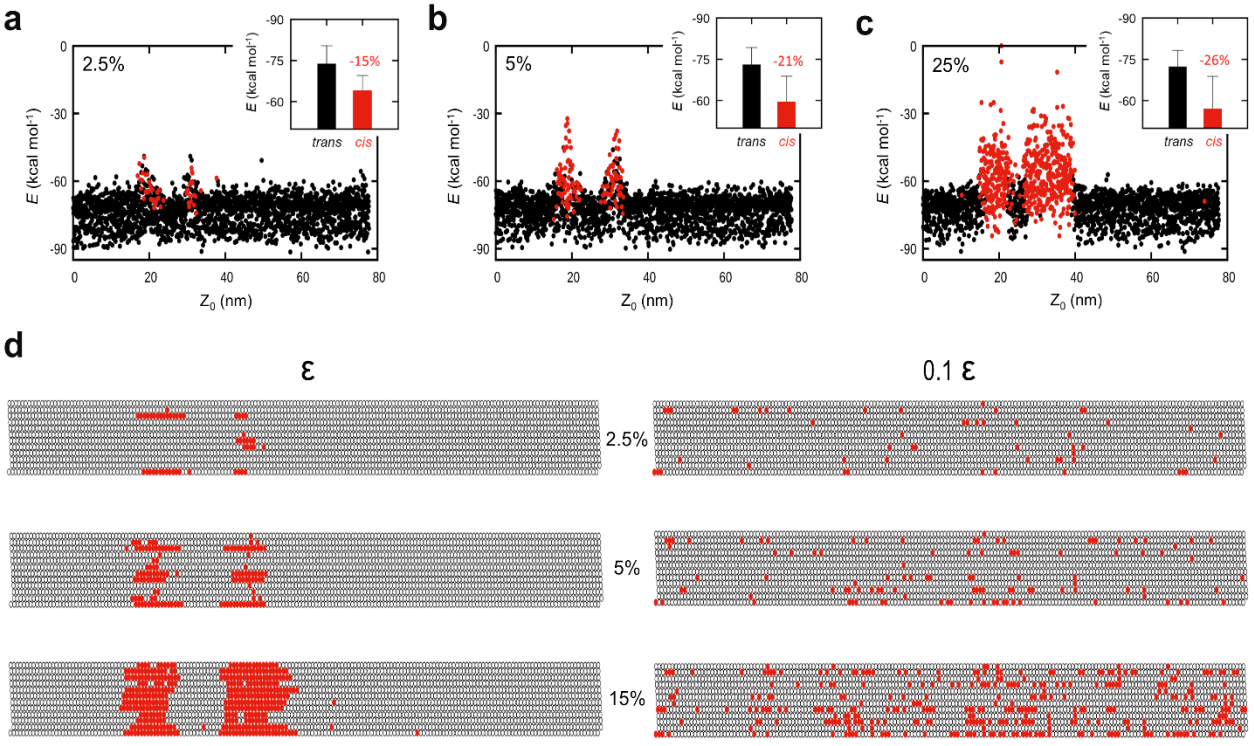

Figure 6 Energy dissipation through defects amplification. **a-c** Interaction energy *E* of each monomer with the other ones in the tubule as a function of the initial *z* position (Z_0) along the tubule at 2.5% (**a**), 5% (**b**) and 25% of *cis* (**c**). *Trans* tails are identified in black, *cis* ones in red. While *trans* monomers globally preserve their average interaction energy *E*, the interaction of the *cis* monomers (defects) decreases as the transitions proceed in the system (energy dissipation through defects amplification). Error bars in the plots represent s.d. **d** Spatial distribution of *cis* tails in the tubule obtained from **CG$_1$**-MD simulations in native condition (monomer-monomer interaction: ε) or when the crowding in the system is reduced (monomer-monomer interaction reduced to ε/10).

Our results prove that when these tubules absorb energy this is not uniformly distributed among all monomers, but it literally blows out from the local defects that are created and amplified on their structure. This is consistent with recent studies on stress relaxation in vitrimers.[63] Our WT-MetaD study demonstrates that this is a kinetic effect, generated by molecular crowding. However,

it is interesting to note that in our case the crowding in the system is intimately related to how strongly the monomers self-assemble.

Therefore, as a final step we artificially decreased in our toy model the effect of crowding by changing the interaction strength between the tails in the assembly (ε), while keeping the same all other interactions and the bias applied to all monomers for the transitions in the system (see **Methods**). At ¾ ε the tubule is still stable, while the spatial correlation between the *cis* defects appearing during the run is reduced compared to the native case (**Supporting Figure 5**). For lower monomer-monomer interaction regimes (*e.g.*, ½ ε), the tubule structure becomes metastable, while the spatial correlation between the defects decreases further. It is interesting to observe what happens for an extreme case with ε/10. **Figure 6d** shows the spatial distribution of *cis* defects spontaneously appearing during the **CG$_1$**-MD simulation (in red) at 2.5%, 5% and 15% of *cis* in the native model (left, ε) or in a model with ε/10. The difference is striking – in the latter case the defects appear as randomly distributed in the system. **Supporting Figure 6** demonstrates that the stronger is the interaction between the monomers in the assembly (ε), the more correlated the defects appear in the system. We obtain a clear relationship between how strong the monomers self-assemble and how defects spontaneously appear and dynamically accumulate on the supramolecular structure. These results are consistent, and help to rationalize and unify, the different behaviors seen in various types of similar assemblies: from the brittle cracking seen in photo-active crystals[64–66] to the stochastic transitions in a solution of disassembled azobenzene-containing monomers or, for example, in less structured assemblies.[24]

Conclusions

Understanding the molecular principles that control the dynamic evolution of a supramolecular system in far from equilibrium conditions is a prime challenge of supramolecular and systems

chemistry. Gaining such a molecular knowledge of how supramolecular systems behave out-of-equilibrium would enable us to rationally design active materials with fascinating bioinspired dynamic properties. However, this typically represents a prohibitively difficult task.

Focusing on a self-assembled tubule that dynamically responds to UV-light irradiation, we combined fine CG models and WT-MetaD simulations to study the transition of the azobenzene-containing monomers in the tubule structure. We found that the *trans*-to-*cis* azobenzene transition is an extremely rare event in a perfect tubule due to the high crowding in the assembly. On the other hands, transitions are way more probable/frequent in the immediate neighborhood of an existing defect. This provides a picture of the mechanism for the dynamic accumulation of the transitions in the system under the exposure to the stimulus leading to the amplification of local defects on the tubule structure.

All our simulations showed that, when they are brought far from the equilibrium, these tubules react by opening local defects in their structure (singularities) rather than by a homogeneous destabilization of the assembled monomers. Such innate out-of-equilibrium behavior is intrinsic in the assembly and it is deep encoded in the structure of the monomers and in how strongly the monomers self-assemble. Our NVE CG-MD simulations prove that when the tubule absorbs energy, the latter is dissipated faster in time if the tubule creates localized/correlated rather than randomly distributed defects.

Recently, it was shown how the intrinsic dynamics of supramolecular polymers (exchange of monomers) originates from defects.[32,38] Interestingly, here we obtain clear evidence of how defects also control the dynamic evolution of an assembly far from the equilibrium. These results shed light on the factors that control the dynamic and responsive properties of such active supramolecular systems. We come out with a general principle showing us how defects, their

emergence and dynamic accumulation in the system determine the brittle *vs.* soft behavior of the supramolecular material in perturbed condition, while obtaining at the same time precious information to learn how to control them.

Methods

AA model

Density functional theory and *ab initio* calculations demonstrated that the most favorable mechanism for *trans*-to-*cis* azobenzene isomerization occurs according to an out-of-plane rotational path involving the torsion of the N–N bond.[46,47] First, we developed an all atom (AA) model for the monomer of **Figure 1a** initially having the azobenzene tails in *trans* configuration (**Figure 2a**). The reference model has been parametrized using the Generalized Amber Force Field (GAFF).[67] The CNNC dihedral potential in the unperturbed azobenzene tails has been set as in **Figure 2a** (black plot), natively having the minimum in the *trans* conformer.[46,47] In the excited *S* trans* tails, this has been then changed by adding a tabulated potential with the functional form of a cosine that differs from zero only in the *trans* region. In this way, the *cis* minimum is unaffected while the *trans* conformer becomes the new maximum in the CNNC dihedral potential, ~53 kcal mol^{-1} higher than the *cis* minimum (**Figure 2a**, blue plot), which corresponds to the first excited state of azobenzene (*S**).[47] In this way, we obtained and AA model for the excited *S* trans* tails (**AA**$_{S^*}$) where the azobenzene tails undergo spontaneous *trans*-to-*cis* transition during an **AA**$_{S^*}$-MD simulation (see **Figure 2a,b**). The transition occurs in the timescale of ~10^{-12}–10^{-11} s of **AA**$_{S^*}$-MD, consistent with the expected timescale for the azobenzene isomerization event.[40]

The out-of-plane transition pathway obtained with model **AA$_{S^*}$** (see **Figure 2c**, black) was found in optimal agreement with the rotational pathway previously obtained by DFT calculations.[47,48]

QM/MM and AA-MD simulations have been recently used to model *trans*-to-*cis* isomerization in azobenzene-containing self-assembled monolayers (SAMs),[40] nanoparticles,[22] vescicles[24] or tubules.[15] In principle, biasing the *cis*-to-*trans* transition (*e.g.*, changing the CNNC dihedral potential as in model **AA$_{S^*}$**) provides a way to observe the transitions on the assembly. However, the limited space and timescales that can be explored at AA level typically provide an over-rigid/brittle representation of the system where the structure of the assembly cannot relax in the correct physical way during the transitions. Thus, we used model **AA$_{S^*}$** as a reference to build an analogously accurate but more dynamic CG model (**CG$_{S^*}$**).

CG model

We developed a CG model for the photo-responsive monomers of **Figure 1a** (**CG$_{S^*}$**) reproducing the correct *trans*-to-*cis* azobenzene transition consistent with model **AA$_{S^*}$.** It is worth noting that a fine CG description was necessary in this case. In fact, an over-simplified CG representation of the monomers and of their transitions (*e.g.*, approximating the *trans*-to-*cis* azobenzene isomerization as occurring on-plane, *etc.*) would not allow to reproduce correctly the mechanism, kinetics and ultimately the effect of the transitions on the self-assembled structure of the tubule. We used the MARTINI force field as a basis to construct our CG model (**Figure 2a**),[68,69] which guarantees a fine enough description of the system and has recently proved a good framework for modeling various types of supramolecular systems.[29,30,32,33,35,38,39,70] Particular attention was devoted to the CG representation of the azobenzene groups and of the CNNC dihedral, to ensure that model **CG$_{S^*}$** could reproduce the out-of-plane *trans*-to-*cis* isomerization trajectory in the correct way. We used only small MARTINI CG beads to avoid size mismatches impairing the

planarity of the structure (important for the formation of the stacked supramolecular tubules). The hydrophilic oligoether chains were parametrized as done previously.[30] The hydrophobic V-shaped part of the monomers was parametrized to best reproduce their dimerization free energy profile in water as obtained using the AA model. This was estimated for both AA and CG models from 4 independent Metadynamics[71] runs (see **Supporting Figure 2**), where we used the distance between the central aromatic rings of the V-shaped tails as the collective variable (CV), a gaussian height of 0.12 kcal mol^{-1}, a sigma of 0.06 nm and a deposition rate of one gaussian every 20000 time steps.

Unperturbed monomers were treated with a version of this CG model where the central CNNC dihedral potential in the azobenzene units was represented by the native black curve of **Figure 2a**. The CNNC dihedral potential was changed as in model $\mathbf{AA}_{\boldsymbol{S}^*}$ (**Figure 2a**: blue curve) to obtain model $\mathbf{CG}_{\boldsymbol{S}^*}$, representing the excited *trans* tails in the monomers. The bonded terms (bonds, angles, *etc.*) were tuned to ensure that model $\mathbf{CG}_{\boldsymbol{S}^*}$ reproduced the correct out-of-plane isomerization trajectory seen of model $\mathbf{AA}_{\boldsymbol{S}^*}$ on the CNNC and CCNN plane and in terms of out-of-plane height of the tail end (see **Figure 2c,d**: blue *vs.* black). Complete parameters for all developed CG monomer models (unperturbed and perturbed) are provided in the **Supporting Information**.

CG model for the unperturbed supramolecular tubule

The starting CG model for the tubule was built as composed of 180 planar hexagonal rings, each containing 6 monomers stacked on the top of each other (see **Figure 1**: scheme) and arranged in such a way to reproduce the AA models for these tubules.[23] The tubule model replicates along *z* direction through the simulation box *via* periodic boundary conditions, effectively modeling a section of ~80 nm of length of an infinite supramolecular tubule (**Figure 3a**). The CG tubule has

been solvated (using standard MARTINI W water) and equilibrated for 3 μs of CG-MD in unperturbed conditions (all monomers with the native CNNC dihedral potential of **Figure 2a**, black, showing great structural stability. The order in the assembly was monitored by an order parameter ϕ,[23] measuring the relative orientation between the monomers. Starting from a value of 1 (initially perfect monomer stacking/arrangement), ϕ readily equilibrates to ~0.96 during the simulation, indicating a highly ordered supramolecular structure in the unperturbed tubule (see **Supporting Figure 3**). The evolution of the order parameter ϕ and of the monomer-monomer interaction energy in the tubule *E* (per-monomer) demonstrates that the tubule stably reached the equilibrium in the CG-MD regime (see **Supporting Figure 3**). Order parameter ϕ was calculated with the PLUMED 2.4 plugin[72] as in our previous work.[23] All vectors representing the relative orientation of the central aromatic ring of each monomer have been calculated using the collective variable PLANES and then used as the input by the collective variable POLYMER_ANGLES to calculate ϕ as the average cosine between neighbor vectors.

WT-MetaD simulations to study monomer transitions in the tubule

As recently done to study rare molecular transitions in supramolecular polymers,[32,38,39] we used WT-MetaD simulations to study the mechanism and kinetics of the monomer transitions in the assembled tubule. First, we conducted WT-MetaD simulations activating (biasing) the transition to *cis* of one (unperturbed) *trans* tail in a perfect tubule. From these runs we obtained information on the native free energy barrier for the process (**Figure 3b**, red). The same WT-MetaD approach was used to qualitatively estimate the barrier to the transition (**Figure 3b**, black) of one (unperturbed) *trans* tail in correspondence (in the immediate neighborhood) of a *cis* defect already present on the structure of the tubule (the configuration of the tubule at 15% of *cis* was used to this end, taken from one of the simulations described in the next section). The results were obtained

from 4 independent WT-MetaD simulations activating the transition for each system, where we used the central CNNC dihedral angle in the azobenzene tail units as the collective variable (CV), a gaussian height of 0.5 kcal mol^{-1}, a sigma of 0.35 rad, a deposition rate of one gaussian every 1000 time steps and bias factor 100.

Next, we assumed one *trans* tail as excited (**CG**$_{S^*}$) in a tubule model where all other *trans* tails were unperturbed. In such a case, the *S* trans* tail does not undergo spontaneous transition in the timescale accessible by a **CG**$_{S^*}$-MD simulation. We used multiple infrequent WT-MetaD simulations to activate (bias) the transition of the *S* tail* to *cis*, and to reconstruct the real (unbiased) kinetics for the event.[32,55] In these runs we used the central CNNC dihedral angle in the excited **CG**$_{S^*}$ azobenzene tail unit as the collective variable (CV), a gaussian height of 0.5 kcal mol^{-1}, a sigma of 0.35 rad, a deposition rate of one gaussian every 4000 time steps and bias factor 50.

The unbiased transition time (t) can be calculated from each infrequent WT-MetaD run as:

$$t = t_{WT-MetaD}\langle e^{\beta(V(s(\mathbf{R}),t))}\rangle_{WT-MetaD} \quad (1)$$

where $V(s(\mathbf{R}),t)$ is the time dependent bias, the bracketed exponential is averaged over the WT-MetaD run and β is kT^{-1}. We used the transition times (t) calculated from 20 independent infrequent WT-MetaD runs (**Figure 3c**: each grey "step" represents the t obtained from one WT-MetaD) to build the transition probability distributions $P_{n\geq 1}$:

$$P_{n\geq 1} = 1 - e^{-\frac{t}{\tau}} \quad (2)$$

where τ is the characteristic timescale for the transition. The $P_{n\geq l}$ distribution was found fitting well with the typical Poisson distribution expected for a rare event, proving the correctness of the adopted setup.[56] The τ is found in the timescale of minutes (~10^1–10^2 s) for the transition of one excited *trans* tail (**CG*S*****) in a perfect tubule. The transition of an excited *trans* tail (**CG*S*****) in the immediate neighborhood of *cis* defects already present on the tubule structure is considerably faster and could be estimated from multiple **CG*S*****-MD simulations (~10^{-11}–10^{-10} s). This is close to the characteristic timescale for the transition in an unconstrained excited disassembled monomer (~10^{-11} s) and in free excited azobenzene. [40,57] These data are also consistent with the free energy barriers obtained from our WT-MetaD runs for non-excited tails (**Figure 3b**). In the latter case, the barrier is very similar to that of the CNNC dihedral of an unperturbed disassembled monomer (**Figure 2a**, black curve). In the former case, the barrier is higher. The difference of ~27 kcal mol^{-1} between the red and black barriers in **Figure 3b** is due to the crowding in the assembly, which makes the transition more rare (slower). As a last check, changing the CNNC dihedral potential term of one excited *trans* tail (**CG*S*****) in the perfect tubule as in the blue curve of **Figure 2a**, but setting the *trans* maximum as high as 67 kcal mol^{-1} (native barrier in the CNNC dihedral potential plus the additional energy necessary to win the crowding) made the transition occurring again in timescale close to the typical one for monomeric excited azobenzene.[40]

Modeling the effect of the transitions on the tubule

We were interested in studying the effect of the *trans*-to-*cis* transitions on the assembly. In the real system the percentage of *cis* tails in the tubules increases on the timescale of minutes.[23] This is imputable to a combination of factors including the low quantum yield of the light-induced excitation, practical limitations in irradiating all the monomers at the same time, the intrinsic

timescale needed for the transitions in the tubule, possible back *cis*-to-*trans* transitions in the real system, *etc.* Modeling the stochastic nature of photo-activated monomer transitions that occur on such a long timescale exceeds the possibility of MD simulations. Thus, we adopted a different approach. If all *trans* tails in the system are considered excited in the tubule (unrealistic case), 100% of *cis* is reached very quickly during the CG-MD run (see **Methods**).[17,33] However, such a simulation setup accelerates too much the transition in the tubule compared to the relaxation time of the assembly. The tubule does not have enough time to equilibrate following to the transitions and appears as over-brittle/rigid. Thus, to obtain a more realistic physical picture of the system, we equilibrated the supramolecular tubule at different percentages of *cis* tails (2.5%, 5%, 10%, 15%, 20% and 30%), which were kept constant during as many CG-MD simulations. These configurations have been then equilibrated/relaxed *via* 5 μs of CG-MD simulations in NPT conditions (constant N: number of particles, P: pressure and T: temperature during the runs). The *cis* percentages in the various systems were kept as fixed during these simulations (*cis* tails have the CNNC dihedral potential described by the blue curve of **Figure 2a**, while the unperturbed *trans* ones by the black one). We then calculated the average energetic (E) and structural impairment (ϕ) of the tubule at the CG-MD equilibrium at the different *cis* percentages (**Figure 3b,c**: black points). These parameters were used to optimize dynamic toy model $\mathbf{CG_1}$ (see below sections).

Energy transformation during the dynamic evolution of the perturbed tubule

Similar simulations at fixed percentage of *cis* – 5% (**Figure 4**), 10% and 15% – were also conducted in NVE conditions (constant N: number of particles, V: volume and E: energy) to study the conversion of the absorbed energy in the system during the out-of-equilibrium evolution of the system. In these runs, we compared the configurations for the tubule used above (correlated

defects) with tubule models where the excited tails were randomly distributed on the structure. The same bias for the transitions was provided to both configurations of the tubule at parity of *cis* percentage, while the unique difference was the distribution of the excited tails. Initially, we described the excited tails with the standard **CG*S**** model, having the *S* trans* ~53 kcal mol^{-1} higher than the native *trans* minimum (**Figure 2a**, black curve). However, in such a case in the tubule model with random distributed *S** tails we could not observe any spontaneous transition (consistent with our WT-MetaD simulations). This demonstrated that in such a condition the transitions require longer time than when these are spatially correlated into local defects on the tubule structure. To further prove this effect, we repeated the analysis by increasing the height the *S* tails* to 67 kcal mol^{-1} (native barrier in the CNNC dihedral potential plus the additional energy necessary to win the crowding). However, also in this case the difference in the dynamic evolution produced by random *vs.* spatially correlated defects was striking (see data in **Figure 4**).

Dynamic toy models

We used these data to build a dynamic model (**CG$_1$**) where the bias on the CNNC dihedral was applied to all monomer tails in the system. The applied bias was optimized to produce on the assembly the same average effect/impairment (structural and energetic) obtained by equilibrating the tubule at increasing (static) percentages of *cis* as described in the previous section (**Figure 5b,c**: red curves *vs.* black points). Thus, model **CG$_1$** does not aim at reproducing anymore the precise physics of the transitions in the assembly, but rather the average behavior of the tubule in a regime where the transitions accumulate on a slow timescale (phenomenological model). In dynamic model **CG$_1$**, the CNNC dihedral potential is described by a simple cosine function with minimum in the *cis* and maximum in the *trans*:

$$V(\varphi) = k(1 + \cos(n\varphi - \varphi_s)) \quad (3)$$

where k = 4.78 kcal mol^{-1}, n = 1 and φ_s = 180°. These values were optimized to obtain a consistent dynamic evolution of the tubule model during a **CG$_1$**-MD simulation (**Figure 5b,c**: red curves *vs.* black points). This was also verified to be the minimal bias necessary to effectively observe the transitions in the tubule in the timescale accessible by a **CG$_1$**-MD, while in this case the *trans*-to-*cis* transitions accumulate slowly enough to leave sufficient time to the supramolecular structure to properly relax and equilibrate (soft behavior). Noteworthy, model **CG$_1$** correctly reproduces the out-of-plane *trans*-to-*cis* transition pathway of excited azobenzene as models **CG$_{S^*}$** and **AA$_{S^*}$** (see **Figure 2c**: red *vs.* black/blue).

Using **CG$_1$** as a toy model, we then decreased the interaction between the V-shaped tails in the tubule to study the effect on the spatial correlation of the dynamically generated *cis* defects. In particular, considered the native MARTINI non-bond interaction (ε) between the CG beads composing the V-shaped tails (SC5 in the original model), we reduced these to ¾ ε, ½ ε and ε/10. As a criterion to distinguish *cis* from *trans* tails in all these simulations, we used a CNNC dihedral angle threshold of 90° (halfway of the *trans*-to-*cis* transition). At ¾ ε the tubules are still persistent (see **Supporting Figure 5**). Although at lower ε regimes these become unstable, the positions of *cis* tails for the ε/10 system were plotted in **Figure 6d** based on their original position in the tubule for comparison.

Simulation parameters

All AA and CG simulations have been performed with the GROMACS 5.1.2 software.[73] The MD simulations to analyze the *trans*-to-*cis* isomerization pathway have been conducted in vacuum and at low temperature (100 K), to reduce the noise and using a time step of 1 fs for both the AA

and the CG system (slow enough to follow the fast transitions). In all simulations we used the V-rescale thermostat to control the temperature,[74] with a coupling time constant of 2 ps. All CG-MD and WT-MetaD simulations of the supramolecular tubule were conducted in water and in NPT conditions using a time step of 15 fs. The simulations were conducted at 300 K of temperature and 1 atm of pressure using the V-rescale thermostat and the Berendsen barostat[75] with semi-isotropic pressure scaling, using a compressibility of $4.5 * 10^{-4}$ MPa^{-1} and a coupling time constant of 2 ps. The CG-MD simulations used to monitor the energy conversion in the system (**Figure 4b-d**) were conducted in NVE conditions using a time step of 10 fs. In the absence of a thermostat, this allowed us to monitor the increase of kinetic energy and temperature in the system.

ASSOCIATED CONTENT

Supporting Information.

The following material is available free of charge on the ACS Publications website. Details and parameters of the molecular models, additional information, data, results and a movie from the molecular simulations (PDF) and Supporting Movie 1.mpg (MPG movie).

AUTHOR INFORMATION

Corresponding Author

*Giovanni M. Pavan. Department of Innovative Technologies, University of Applied Sciences and Arts of Southern Switzerland, Galleria 2, Via Cantonale 2c, CH-6928 Manno, Switzerland. Email: giovanni.pavan@supsi.ch

Author Contributions

G.M.P. conceived this work, designed the computational strategy and supervised the work. D.B. performed the modeling and simulation work. S.K. and T.K. contributed the experimental results. All authors analyzed and discussed the results, and contributed to the writing of this manuscript.

ACKNOWLEDGMENTS

The authors acknowledge the support from the Swiss National Science Foundation (SNSF grant 200021_175735 to G.M.P.).

REFERENCES

(1) Kinbara, K.; Aida, T. Toward Intelligent Molecular Machines: Directed Motions of Biological and Artificial Molecules and Assemblies. *Chem. Rev.* **2005**, *105*, 1377–1400.

(2) Simons, K.; Ikonen, E. Functional Rafts in Cell Membranes. *Nature* **1997**, *387*, 569–572.

(3) Mofrad, M. R. K.; Kamm, R. D. *Cytoskeletal Mechanics: Models and Measurements in Cell Mechanics*; Cambridge University Press, 2006; Vol. 9780521846.

(4) Howard, J.; Hyman, A. A. Dynamics and Mechanics of the Microtubule plus End. *Nature* **2003**, *422*, 753–758.

(5) Grishchuk, E. L.; Molodtsov, M. I.; Ataullakhanov, F. I.; McIntosh, J. R. Force Production by Disassembling Microtubules. *Nature* **2005**, *438*, 384–388.

(6) Molodtsov, M. I.; Grishchuk, E. L.; Efremov, A. K.; McIntosh, J. R.; Ataullakhanov, F. I. Force Production by Depolymerizing Microtubules: A Theoretical Study. *Proc. Natl. Acad. Sci. U. S. A.* **2005**, *102*, 4353–4358.

(7) Boyer, P. D. The ATP Synthase - a Splendid Molecular Machine. *Annu. Rev. Biochem.* **1997**, *66*, 717–749.

(8) Sun, L.; Huang, W. M.; Ding, Z.; Zhao, Y.; Wang, C. C.; Purnawali, H.; Tang, C. Stimulus-Responsive Shape Memory Materials: A Review. *Mater. Des.* **2012**, *33*, 577–640.

(9) Hariadi, R. F.; Sommese, R. F.; Adhikari, A. S.; Taylor, R. E.; Sutton, S.; Spudich, J. A.; Sivaramakrishnan, S. Mechanical Coordination in Motor Ensembles Revealed Using Engineered Artificial Myosin Filaments. *Nat. Nanotechnol.* **2015**, *10*, 696–700.

(10) Abendroth, J. M.; Bushuyev, O. S.; Weiss, P. S.; Barrett, C. J. Controlling Motion at the Nanoscale: Rise of the Molecular Machines. *ACS Nano* **2015**, *9*, 7746–7768.

(11) Koumura, N.; Zijistra, R. W. J.; Van Delden, R. A.; Harada, N.; Feringa, B. L. Light-Driven Monodirectional Molecular Rotor. *Nature* **1999**, *401*, 152–155.

(12) Bissell, R. A.; Córdova, E.; Kaifer, A. E.; Stoddart, J. F. A Chemically and Electrochemically Switchable Molecular Shuttle. *Nature* **1994**, *369*, 133–137.

(13) Kudernac, T.; Ruangsupapichat, N.; Parschau, M.; MacIá, B.; Katsonis, N.; Harutyunyan, S. R.; Ernst, K. H.; Feringa, B. L. Electrically Driven Directional Motion of a Four-Wheeled Molecule on a Metal Surface. *Nature* **2011**, *479*, 208–211.

(14) Kassem, S.; van Leeuwen, T.; Lubbe, A. S.; Wilson, M. R.; Feringa, B. L.; Leigh, D. A.

Artificial Molecular Motors. *Chem. Soc. Rev.* **2017**, *46*, 2592–2621.

(15) Wilson, M. R.; Solà, J.; Carlone, A.; Goldup, S. M.; Lebrasseur, N.; Leigh, D. A. An Autonomous Chemically Fuelled Small-Molecule Motor. *Nature* **2016**, *534*, 235–240.

(16) Balzani, V.; Credi, A.; Venturi, M. Light Powered Molecular Machines. *Chem. Soc. Rev.* **2009**, *38*, 1542.

(17) Astumian, R. D. Stochastically Pumped Adaptation and Directional Motion of Molecular Machines. *Proc. Natl. Acad. Sci. U. S. A.* **2018**, *115*, 9405–9413.

(18) Mishra, A.; Korlepara, D. B.; Kumar, M.; Jain, A.; Jonnalagadda, N.; Bejagam, K. K.; Balasubramanian, S.; George, S. J. Biomimetic Temporal Self-Assembly *via* Fuel-Driven Controlled Supramolecular Polymerization. *Nat. Commun.* **2018**, *9*, 1295.

(19) Bandara, H. M. D.; Burdette, S. C. Photoisomerization in Different Classes of Azobenzene. *Chem. Soc. Rev.* **2012**, *41*, 1809–1825.

(20) Yagai, S.; Iwai, K.; Yamauchi, M.; Karatsu, T.; Kitamura, A.; Uemura, S.; Morimoto, M.; Wang, H.; Würthner, F. Photocontrol over Self-Assembled Nanostructures of π-π Stacked Dyes Supported by the Parallel Conformer of Diarylethene. *Angew. Chem. Int. Ed.* **2014**, *53*, 2602–2606.

(21) Dohno, C.; Uno, S. N.; Nakatani, K. Photoswitchable Molecular Glue for DNA. *J. Am. Chem. Soc.* **2007**, *129*, 11898–11899.

(22) Zhao, H.; Sen, S.; Udayabhaskararao, T.; Sawczyk, M.; Kucanda, K.; Manna, D.; Kundu, P. K.; Lee, J. W.; Král, P.; Klajn, R. Reversible Trapping and Reaction Acceleration within

Dynamically Self-Assembling Nanoflasks. *Nat. Nanotechnol.* **2016**, *11*, 82–88.

(23) Fredy, J. W.; Méndez-Ardoy, A.; Kwangmettatam, S.; Bochicchio, D.; Matt, B.; Stuart, M. C. A.; Huskens, J.; Katsonis, N.; Pavan, G. M.; Kudernac, T. Molecular Photoswitches Mediating the Strain-Driven Disassembly of Supramolecular Tubules. *Proc. Natl. Acad. Sci. U. S. A.* **2017**, *114*, 11850–11855.

(24) Molla, M. R.; Rangadurai, P.; Antony, L.; Swaminathan, S.; De Pablo, J. J.; Thayumanavan, S. Dynamic Actuation of Glassy Polymersomes through Isomerization of a Single Azobenzene Unit at the Block Copolymer Interface. *Nat. Chem.* **2018**, *10*, 659–666.

(25) Astumian, R. D. Optical: Vs. Chemical Driving for Molecular Machines. *Faraday Discuss.* **2016**, *195*, 583–597.

(26) Astumian, R. D. How Molecular Motors Work-Insights from the Molecular Machinist's Toolbox: The Nobel Prize in Chemistry 2016. *Chem. Sci.* **2017**, *8*, 840–845.

(27) Astumian, R. D. Trajectory and Cycle-Based Thermodynamics and Kinetics of Molecular Machines: The Importance of Microscopic Reversibility. *Acc. Chem. Res*. **2018**, *51*, 2653–2661.

(28) Garzoni, M.; Baker, M. B.; Leenders, C. M. A.; Voets, I. K.; Albertazzi, L.; Palmans, A. R. A.; Meijer, E. W.; Pavan, G. M. Effect of H-Bonding on Order Amplification in the Growth of a Supramolecular Polymer in Water. *J. Am. Chem. Soc.* **2016**, *138*, 13985–13995.

(29) Bochicchio, D.; Pavan, G. M. Molecular Modelling of Supramolecular Polymers. *Adv. Phys. X* **2018**, *3*, 1436408.

(30) Bochicchio, D.; Pavan, G. M. From Cooperative Self-Assembly to Water-Soluble Supramolecular Polymers Using Coarse-Grained Simulations. *ACS Nano* **2017**, *11*, 1000–1011.

(31) Bochicchio, D.; Pavan, G. M. Effect of Concentration on the Supramolecular Polymerization Mechanism *via* Implicit-Solvent Coarse-Grained Simulations of Water-Soluble 1,3,5-Benzenetricarboxamide. *J. Phys. Chem. Lett.* **2017**, *8*, 3813–3819.

(32) Bochicchio, D.; Salvalaglio, M.; Pavan, G. M. Into the Dynamics of a Supramolecular Polymer at Submolecular Resolution. *Nat. Commun.* **2017**, *8*, 147.

(33) Lee, O. S.; Cho, V.; Schatz, G. C. Modeling the Self-Assembly of Peptide Amphiphiles into Fibers Using Coarse-Grained Molecular Dynamics. *Nano Lett.* **2012**, *12*, 4907–4913.

(34) Bejagam, K. K.; Balasubramanian, S. Supramolecular Polymerization: A Coarse Grained Molecular Dynamics Study. *J. Phys. Chem. B* **2015**, *119*, 5738–5746.

(35) Casellas, N. M.; Pujals, S.; Bochicchio, D.; Pavan, G. M.; Torres, T.; Albertazzi, L.; García-Iglesias, M. From Isodesmic to Highly Cooperative: Reverting the Supramolecular Polymerization Mechanism in Water by Fine Monomer Design. *Chem. Commun.* **2018**, *54*, 4112–4115.

(36) Amado Torres, D.; Garzoni, M.; Subrahmanyam, A. V.; Pavan, G. M.; Thayumanavan, S. Protein-Triggered Supramolecular Disassembly: Insights Based on Variations in Ligand Location in Amphiphilic Dendrons. *J. Am. Chem. Soc.* **2014**, *136*, 5385–5399.

(37) Molla, M. R.; Rangadurai, P.; Pavan, G. M.; Thayumanavan, S. Experimental and

Theoretical Investigations in Stimuli Responsive Dendrimer-Based Assemblies. *Nanoscale* **2015**, *7*, 3817–3837.

(38) Torchi, A.; Bochicchio, D.; Pavan, G. M. How the Dynamics of a Supramolecular Polymer Determines Its Dynamic Adaptivity and Stimuli-Responsiveness: Structure–Dynamics–Property Relationships From Coarse-Grained Simulations. *J. Phys. Chem. B* **2018**, *122*, 4169–4178.

(39) Jung, S. H.; Bochicchio, D.; Pavan, G. M.; Takeuchi, M.; Sugiyasu, K. A Block Supramolecular Polymer and Its Kinetically Enhanced Stability. *J. Am. Chem. Soc.* **2018**, *140*, 10570–10577.

(40) Cantatore, V.; Granucci, G.; Rousseau, G.; Padula, G.; Persico, M. Photoisomerization of Self-Assembled Monolayers of Azobiphenyls: Simulations Highlight the Role of Packing and Defects. *J. Phys. Chem. Lett.* **2016**, *7*, 4027–4031.

(41) Ilnytskyi, J. M.; Slyusarchuk, A.; Saphiannikova, M. Photocontrollable Self-Assembly of Azobenzene-Decorated Nanoparticles in Bulk: Computer Simulation Study. *Macromolecules* **2016**, *49*, 9272–9282.

(42) Stoffelen, C.; Voskuhl, J.; Jonkheijm, P.; Huskens, J. Dual Stimuli-Responsive Self-Assembled Supramolecular Nanoparticles. *Angew. Chem. Int. Ed.* **2014**, *53*, 3400–3404.

(43) Peter, C.; Delle Site, L.; Kremer, K. Classical Simulations from the Atomistic to the Mesoscale and Back: Coarse Graining an Azobenzene Liquid Crystal. *Soft Matter* **2008**, *4*, 859–869.

(44) Böckmann, M.; Peter, C.; Site, L. D.; Doltsinis, N. L.; Kremer, K.; Marx, D. Atomistic Force Field for Azobenzene Compounds Adapted for QM/MM Simulations with Applications to Liquids and Liquid Crystals. *J. Chem. Theory Comput.* **2007**, *3*, 1789–1802.

(45) Li, Z.; Wang, P.; Liu, B.; Wang, Y.; Zhang, J.; Yan, Y.; Ma, Y. Unusual, Photo-Induced Self-Assembly of Azobenzene-Containing Amphiphiles. *Soft Matter* **2014**, *10*, 8758–8764.

(46) Pederzoli, M.; Pittner, J.; Barbatti, M.; Lischka, H. Nonadiabatic Molecular Dynamics Study of the *Cis-Trans* Photoisomerization of Azobenzene Excited to the S_1 State. *J. Phys. Chem. A* **2011**, *115*, 11136–11143.

(47) Tiago, M. L.; Ismail-Beigi, S.; Louie, S. G. Photoisomerization of Azobenzene from First-Principles Constrained Density-Functional Calculations. *J. Chem. Phys.* **2005**, *122*, 094311.

(48) Crecca, C. R.; Roitberg, A. E. Theoretical Study of the Isomerization Mechanism of Azobenzene and Disubstituted Azobenzene Derivatives. *J. Phys. Chem. A* **2006**, *110*, 8188–8203.

(49) Barducci, A.; Bussi, G.; Parrinello, M. Well-Tempered Metadynamics: A Smoothly Converging and Tunable Free-Energy Method. *Phys. Rev. Lett.* **2008**, *100*, 020603.

(50) Pace, G.; Ferri, V.; Grave, C.; Elbing, M.; von Hanisch, C.; Zharnikov, M.; Mayor, M.; Rampi, M. A.; Samori, P. Cooperative Light-Induced Molecular Movements of Highly Ordered Azobenzene Self-Assembled Monolayers. *Proc. Natl. Acad. Sci. U. S. A.* **2007**, *104*, 9937–9942.

(51) Titov, E.; Granucci, G.; Götze, J. P.; Persico, M.; Saalfrank, P. Dynamics of Azobenzene

Dimer Photoisomerization: Electronic and Steric Effects. *J. Phys. Chem. Lett.* **2016**, *7*, 3591–3596.

(52) Tirosh, E.; Benassi, E.; Pipolo, S.; Mayor, M.; Valásek, M.; Frydman, V.; Corni, S.; Cohen, S. R. Direct Monitoring of Opto-Mechanical Switching of Self-Assembled Monolayer Films Containing the Azobenzene Group. *Beilstein J. Nanotechnol.* **2011**, *2*, 834–844.

(53) Akiyama, H.; Tamada, K.; Nagasawa, J.; Abe, K.; Tamaki, T. Photoreactivity in Self-Assembled Monolayers Formed from Asymmetric Disulfides Having Para-Substituted Azobenzenes. *J. Phys. Chem. B* **2003**, *107*, 130–135.

(54) Samanta, D.; Gemen, J.; Chu, Z.; Diskin-Posner, Y.; Shimon, L. J. W.; Klajn, R. Reversible Photoswitching of Encapsulated Azobenzenes in Water. *Proc. Natl. Acad. Sci. U. S. A.* **2018**, *115*, 9379–9384.

(55) Tiwary, P.; Parrinello, M. From Metadynamics to Dynamics. *Phys. Rev. Lett.* **2013**, *111*, 230602.

(56) Salvalaglio, M.; Tiwary, P.; Parrinello, M. Assessing the Reliability of the Dynamics Reconstructed from Metadynamics. *J. Chem. Theory Comput.* **2014**, *10*, 1420–1425.

(57) Stuart, C. M.; Frontiera, R. R.; Mathies, R. A. Excited-State Structure and Dynamics of Cis- and Trans-Azobenzene from Resonance Raman Intensity Analysis. *J. Phys. Chem. A* **2007**, *111*, 12072–12080.

(58) England, J. L. Dissipative Adaptation in Driven Self-Assembly. *Nat. Nanotechnol.* **2015**, *10*, 919–923.

(59) Te Brinke, E.; Groen, J.; Herrmann, A.; Heus, H. A.; Rivas, G.; Spruijt, E.; Huck, W. T. S. Dissipative Adaptation in Driven Self-Assembly Leading to Self-Dividing Fibrils. *Nat. Nanotechnol.* **2018**, *13*, 849–855.

(60) Boekhoven, J.; Brizard, A. M.; Kowlgi, K. N. K.; Koper, G. J. M.; Eelkema, R.; Van Esch, J. H. Dissipative Self-Assembly of a Molecular Gelator by Using a Chemical Fuel. *Angew. Chem. Int. Ed.* **2010**, *49*, 4825–4828.

(61) della Sala, F.; Neri, S.; Maiti, S.; Chen, J. L.-Y.; Prins, L. J. Transient Self-Assembly of Molecular Nanostructures Driven by Chemical Fuels. *Curr. Opin. Biotechnol.* **2017**, *46*, 27–33.

(62) Astumian, R. D. Stochastic Pumping of Non-Equilibrium Steady-States: How Molecules Adapt to a Fluctuating Environment. *Chem. Commun.* **2017**, *54*, 427–444.

(63) Ciarella, S.; Sciortino, F.; Ellenbroek, W. G. Dynamics of Vitrimers: Defects as a Highway to Stress Relaxation. *Phys. Rev. Lett.* **2018**, *121*, 058003.

(64) Panda, M. K.; Ghosh, S.; Yasuda, N.; Moriwaki, T.; Mukherjee, G. D.; Reddy, C. M.; Naumov, P. Spatially Resolved Analysis of Short-Range Structure Perturbations in a Plastically Bent Molecular Crystal. *Nat. Chem.* **2015**, *7*, 65–72.

(65) Nath, N. K.; Runčevski, T.; Lai, C. Y.; Chiesa, M.; Dinnebier, R. E.; Naumov, P. Surface and Bulk Effects in Photochemical Reactions and Photomechanical Effects in Dynamic Molecular Crystals. *J. Am. Chem. Soc.* **2015**, *137*, 13866–13875.

(66) Lai, C. Y.; Raj, G.; Liepuoniute, I.; Chiesa, M.; Naumov, P. Direct Observation of

Photoinduced Trans-Cis Isomerization on Azobenzene Single Crystal. *Cryst. Growth Des.* **2017**, *17*, 3306–3312.

(67) Wang, J.; Wolf, R. M.; Caldwell, J. W.; Kollman, P. A.; Case, D. A. Development and Testing of a General Amber Force Field. *J. Comput. Chem.* **2004**, *25*, 1157–1174.

(68) Marrink, S. J.; de Vries, A. H.; Mark, A. E. Coarse Grained Model for Semiquantitative Lipid Simulations. *J. Phys. Chem. B* **2004**, *108*, 750–760.

(69) Marrink, S. J.; Risselada, H. J.; Yefimov, S.; Tieleman, D. P.; De Vries, A. H. The MARTINI Force Field: Coarse Grained Model for Biomolecular Simulations. *J. Phys. Chem. B* **2007**, *111*, 7812–7824.

(70) Frederix, P. W. J. M.; Patamanidis, I.; Marrink, S. J. Bio-Inspired Supramolecular Systems and Their Connection to Experiments. *Chem. Soc. Rev.* **2018**, *47*, 3470–3489.

(71) Laio, A.; Parrinello, M. Escaping Free-Energy Minima. *Proc. Natl. Acad. Sci. U. S. A.* **2002**, *99*, 12562–12566.

(72) Tribello, G. A.; Bonomi, M.; Branduardi, D.; Camilloni, C.; Bussi, G. PLUMED 2: New Feathers for an Old Bird. *Comput. Phys. Commun.* **2014**, *185*, 604–613.

(73) Abraham, M. J.; Murtola, T.; Schulz, R.; Páall, S.; Smith, J. C.; Hess, B.; Lindah, E. Gromacs: High Performance Molecular Simulations through Multi-Level Parallelism from Laptops to Supercomputers. *SoftwareX* **2015**, *1–2*, 19–25.

(74) Bussi, G.; Donadio, D.; Parrinello, M. Canonical Sampling through Velocity Rescaling. *J. Chem. Phys.* **2007**, *126*, 014101.

(75) Berendsen, H. J. C.; Postma, J. P. M.; Van Gunsteren, W. F.; Dinola, A.; Haak, J. R. Molecular Dynamics with Coupling to an External Bath. *J. Chem. Phys.* **1984**, *81*, 3684–3690.

SYNOPSIS (Word Style “SN_Synopsis_TOC”).